Synergising Machine Learning and Remote Sensing for Urban Heat Island Dynamics: A Comprehensive Modelling Approach

atmosphere

MDPI

Article

Synergising Machine Learning and Remote Sensing for Urban Heat Island Dynamics: A Comprehensive Modelling Approach

Guglielmina Mutani [1,*], Alessandro Scalise [2], Xhoana Sufa [2] and Stefania Grasso [3]

[1] Department of Energy, Politecnico di Torino, 10129 Turin, Italy
[2] Planet Smart City, 10129 Turin, Italy; a.scalise@planetsmartcity.com (A.S.); x.sufa@planetsmartcity.com (X.S.)
[3] Metropolitan City of Turin, 10129 Turin, Italy; stefania.grasso@cittametropolitana.torino.it (S.G.)
* Correspondence: guglielmina.mutani@polito.it

Abstract: This study evaluates the effectiveness of sustainable urban regeneration projects in mitigating Urban Heat Island (UHI) effects through a place-based approach. Geographic Information Systems (GIS) and satellite imagery were integrated with machine learning (ML) models to analyse the urban environment, human activities, and climate data in Turin, Italy. A detailed analysis of the ex-industrial Teksid area revealed a significant reduction in Surface Urban Heat Island Intensity (SUHII), with decreases of −0.94 in summer and −0.54 in winter following regeneration interventions. Using 17 variables in the Random Forest model, key determinants influencing SUHII were identified, including building density, vegetation cover, and surface albedo. This study quantitatively highlights the impact of increasing green spaces and enhancing surface materials to improve solar reflectivity, with findings showing a 19.46% increase in vegetation and a 3.09% rise in albedo after mitigation efforts. Furthermore, the results demonstrate that integrating Local Climate Zones (LCZs) into urban planning, alongside interventions targeting these key variables, can further optimise UHI mitigation and assess changes. This comprehensive approach provides policymakers with a robust tool to enhance urban resilience and guide sustainable planning strategies in response to climate change.

Keywords: Urban Heat Islands (UHIs); Surface Urban Heat Island (SUHI); remote sensing; Geographic Information System (GIS); machine learning (ML); Local Climate Zones (LCZs); urban planning

Citation: Mutani, G.; Scalise, A.; Sufa, X.; Grasso, S. Synergising Machine Learning and Remote Sensing for Urban Heat Island Dynamics: A Comprehensive Modelling Approach. *Atmosphere* **2024**, *15*, 1435. https://doi.org/10.3390/atmos15121435

Academic Editors: Francesca Despini, Sofia Costanzini and Shady Attia

Received: 19 September 2024
Revised: 28 October 2024
Accepted: 14 November 2024
Published: 29 November 2024

1. Introduction

The Urban Heat Island (UHI) effect is a well-documented phenomenon wherein urban areas experience elevated temperatures compared to their rural surroundings. This temperature difference arises primarily from the concentration of buildings, infrastructure, and human activities, which alters the natural energy balance of urban environments. The UHI effect exacerbates problems, such as increased energy consumption, air pollution, and adverse health impacts, particularly during extreme weather events. These issues are further amplified by climate change, making UHI mitigation a critical focus for urban planning and environmental policy [1,2].

Oke [3], a pioneer in UHI research, advanced this understanding by distinguishing two layers affected by urbanisation: the Urban Canopy Layer (UCL), influenced by the built environment, and the Urban Boundary Layer (UBL), which extends above the UCL. UHIs can be measured through air temperature sensors for the UCL, thereby capturing Canopy Urban Heat Island (CUHI) effects, or through thermal remote sensing for the UBL, which measures Surface Urban Heat Island (SUHI) intensity [4,5].

As urban areas expand, the boundaries between urban and rural regions have become less distinct, thus complicating traditional UHI assessments. To address this challenge, Oke and Stewart [6,7] developed the Local Climate Zone (LCZ) classification, identifying 17 zones based on built geometries and land cover. Their research established a strong correlation between settlement size—measured based on population and human activity—and UHI intensity [8].

Urban regeneration projects have emerged as effective strategies for mitigating UHIs, particularly when combined with advanced analytical tools, such as Geographic Information Systems (GIS), remote sensing, and machine learning (ML). These technologies allow for comprehensive analysis by integrating spatial, environmental, and socio-economic data [9–13]. Surface Urban Heat Island Intensity (SUHII) offers a detailed understanding of how urban morphology and land use affect heat distribution at the surface level. Recent advancements in remote sensing [14–17] and ML have enabled the creation of more accurate models to predict UHI dynamics. ML algorithms, such as Random Forest, are particularly effective at identifying key variables that influence SUHII, including vegetation cover, building density, and surface albedo [18–23]. The LCZ classification is used to spatially analyse these variables by dividing urban areas into zones based on their physical and thermal properties, making it a valuable tool for targeted urban planning [17,20].

Building on this foundation, resumed in Appendix A, this study focuses on the city of Turin in northwest Italy through an in-depth analysis of the former industrial Teksid area. To comprehensively analyse the urban environment, GIS data and remote sensing imagery were employed to construct a geodatabase. These tools provided insights into the distribution, evolution, and drivers of SUHII by integrating data from multiple sources to develop a place-based model. ML techniques were then applied to assess the complex relationships between SUHII and urban factors, such as geometry, land use, and materials, thus uncovering patterns that traditional methods may have missed.

The LCZ method was also incorporated to assess the settlement morphologies defined by the Regional Landscape Plan (RLP) of the Piedmont Region. This combined approach offered a deeper understanding of SUHII variations based on urban morphologies and provided a comprehensive framework for urban planners to analyse SUHI. By assembling a geo-package for Turin, key variables influencing SUHII were identified, and non-linear relationships between these variables and SUHII were explored through the ML algorithm. Additionally, SUHII patterns were compared with LCZ morphologies to contextualise the findings and enhance our understanding of UHI behaviour across different urban forms.

This integrated approach not only identifies the key drivers of SUHII but also quantifies the impact of mitigation measures and compensatory solutions in critical urban contexts. It provides urban planners with actionable insights for implementing targeted UHI mitigation strategies, particularly in areas constrained by regulations or historical preservation requirements.

2. Materials and Methods

The methodology adopted in this study, as outlined in Figure 1, integrates four key elements guided by the state of the art, which is detailed in Appendix A. These elements include (i) a place-based analysis using GIS to geo-localise and describe urban characteristics [10–14]; (ii) the use of remote sensing imagery to complement the description of the urban environment and assess SUHII [15–18]; (iii) a data-driven model employing ML to analyse SUHII dynamics [19–24]; and (iv) the LCZ method to categorise typical urban contexts and propose mitigation strategies for UHI effects. This combination of approaches provides a comprehensive framework for studying UHI phenomena, thus offering insights that have not been previously integrated into a single methodology.

In the *pre-modelling* phase, GIS and remote sensing data were integrated to build a detailed geodatabase capturing the spatial–temporal variability in Turin during the years 2000–2001 and 2018; environmental indicators were calculated during pre-processing. These data were spatialised and organised into a geo-package for further analysis, thus ensuring consistency across the variables. The pre-processing steps also involved cleaning the data and preparing the data for the modelling stage.

In the *modelling* phase, the Random Forest ML algorithm was chosen due to its robustness against overfitting and ease of integration into the ArcGIS Pro environment. The algorithm was applied to simulate SUHII based on identified key variables. Sensitivity analyses were conducted to identify the most SUHI-related factors. Hyperparameter tuning optimised the model's performance, and the results were calibrated to improve prediction accuracy.

Lastly, the LCZ method was integrated to explore the relationship between urban morphologies and SUHII, thus providing insights into how specific urban forms impact heat distribution. By comparing SUHII with LCZ characteristics, this method allowed for the identification of mitigation measures tailored to different urban morphologies, thus enhancing the potential of effective UHI mitigation strategies.

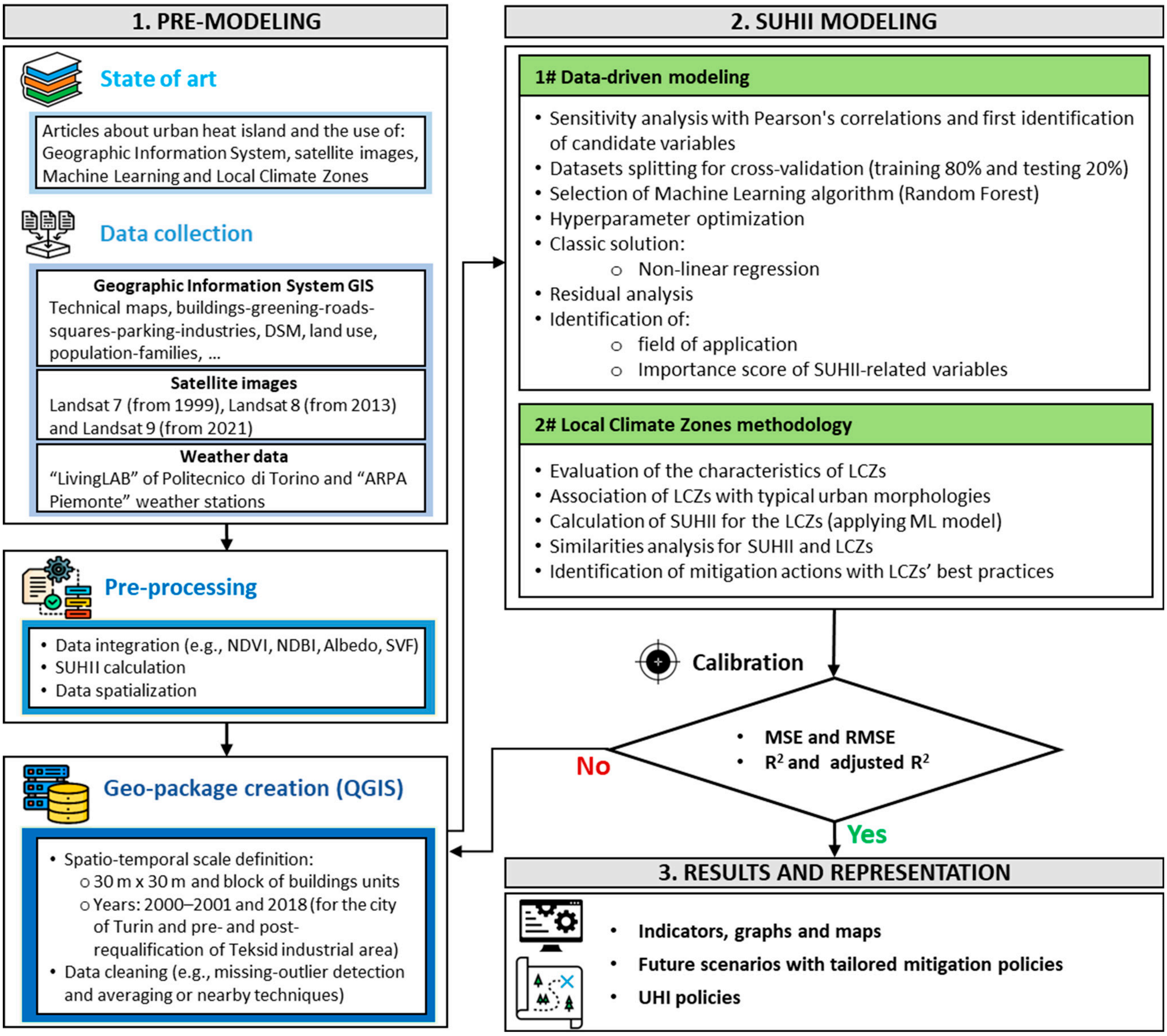

Figure 1. Flowchart of the methodology used to evaluate UHI effects.

2.1. Investigation Area

Turin has historically played a significant industrial role in Italy, particularly as a major hub for automotive manufacturing, with Fiat's production facilities being prominent. This industrial legacy has profoundly influenced the city's urban landscape and contributed to its economic growth. In recent years, Turin has undergone substantial transformation, with numerous regeneration initiatives aimed at revitalising the urban areas once dominated by industry. These interventions have focused on repurposing former industrial sites and integrating green spaces, and they have adopted various strategies to improve liveability, reduce pollution, and promote cultural and recreational amenities, signalling a shift towards a more sustainable and resilient urban environment [25-27].

A key example of these regeneration efforts is the former Teksid area, located in the northern part of the city (as shown in Figure 2). The selection of this site was driven by the need to investigate UHI dynamics within the broader framework of urban regeneration. The Teksid area has undergone extensive redevelopment since its closure in 1992, aligning with the city's overall efforts to revitalise former industrial sites and promote sustainable urban growth [28,29].

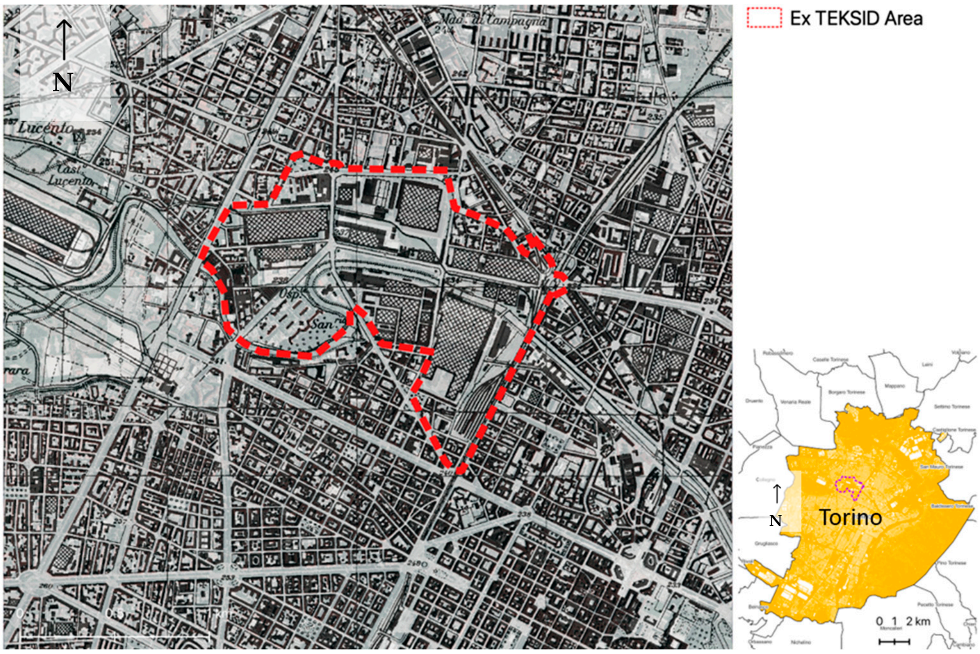

Figure 2. Technical cartography plant (1955–1969), City of Turin.

Focusing on the specific Teksid area allows for a detailed investigation of how previous land uses (Figure 3a) and subsequent post-industrial regeneration efforts (Figure 3b) influence local climate patterns and Urban Heat Island (UHI) effects.

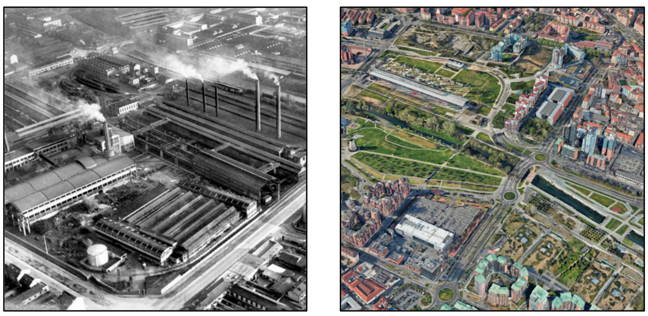

(**a**) (**b**)

Figure 3. (**a**) Former industrial Teksid area in Turin, 1920 (Immagini del cambiamento, archivio CDS5, https://areeweb.polito.it/imgdc/schede/PD04.html). (**b**) Regeneration program in Spina 3. Google Cartographical Data, 2018.

2.2. Data Collection and Pre-Processing

The data for the city of Turin were organised into a comprehensive geo-dataset based on the following sources:

- Buildings, rivers, parks, greenings, public spaces, squares, parking areas, roads, etc.: BDTRE (Banca Dati Territoriale di Riferimento degli Enti, in Italian) 2018, https://www.geoportale.piemonte.it/geonetwork/srv/ita/catalog.search#/search?any=BDTRE, and the municipal technical map of Torino CTC 1999 (Carta Tecnica Comunale, in Italian), http://geoportale.comune.torino.it/geocatalogocoto/?sezione=catalogo; EAGLE (https://eagle-science.org/about/).
- Land use: Corine land cover 2000 and 2018: https://land.copernicus.eu/en/products/corine-land-cover/cha-2000-2006; https://land.copernicus.eu/en/products/corine-land-cover/clc2018.
- Population and families in 2001, 2011, and 2021 from the National Institute of Statistics (ISTAT in Italian): https://www.istat.it/notizia/aggiornamento-basi-territoriali-2021-2/.
- Climate data: weather station of Politecnico di Torino collected by the LivingLAB: https://smartgreenbuilding.polito.it/; other weather stations in Turin: https://www.arpa.piemonte.it/rischi_naturali/snippets_arpa_graphs/map_meteoweb/?rete=stazione_meteorologica.

Satellite image collection was facilitated through the "STAC API Browser" plugin in QGIS [30]. The pre-processing phase involved using the "Semi-Automatic Classification Plugin" (SCP), which handled radiometric, geometric, and atmospheric correction as well as cloud masking tasks [31,32]. The SCP greatly enhances the accuracy, reliability, and interpretability of raw satellite imagery.

The selected images (in Table 1) span the period when the industrial landscape was dominant, starting from 2000 to 2001, which provides a historical baseline. To capture recent urban regeneration initiatives in the pre-COVID-19 era, images from 2018 were used. This minimises anomalies due to the pandemic's impact on human activities, with both years sharing similar climatic conditions. Table 1 highlights the comparable air temperatures and cloud cover for these years, thus strengthening the analysis's comparability. Additionally, seasonal variation was considered by selecting typical days in winter, summer, and transitional seasons to ensure methodological rigour.

Table 1. Selection of Landsat 7 (for typical days in 2000 and 2001) and Landsat 8 (for typical days in 2018) satellite images for the City of Turin.

Landsat Product ID	Date	Time	Cloud Cover -	Cell size m	Season	Air Temp. °C
LC08_L2SP_195029_20180822_20200831_02_T1	11 August 2018	10:16	0.31	30	Summer	26.2
LC08_L2SP_195029_20180211_20200902_02_T1	22 February 2018	10:17	0.23	30	Winter	3.8
LC08_L2SP_195029_20180416_20200901_02_T1	16 April 2018	10:16	0.30	30	Mid-season	17.9
LE07_L1TP_194029_20010824_20200917_02_T1	24 August 2001	09:59	0.04	30	Summer	26.1
LE07_L1TP_195029_20001218_20211122_02_T1	18 December 2000	10:07	0.05	30	Winter	2.1
LE07_L1TP_195029_20010527_20200917_02_T1	27 May 2001	10:07	0.10	30	Mid-season	23.2

2.3. Candidate Variables

A sensitivity analysis in the pre-modelling phase identified candidate variables for subsequent modelling, with the formulas and references in Table 2. Most variables were computed using the "Raster Calculator" tool in QGIS, while others, like the Sky View Factor and building density, were derived from BDTRE and processed with QGIS plugins [33,34].

To automate the analysis, Python scripts in the QGIS Python console were used to compute each variable in Table 2. This involved six Landsat images from three seasonal days in 2001 and 2018, covering all census sections, and 30 m × 30 m cells (144,826 cells total) in Turin. The scripts in Python enable the automatic execution by modifying file paths for Landsat bands; these scripts are available at the link: https://1drv.ms/b/c/8e7ec8768139e3da/EQ_IikuGRxhNrBo6ArS2j7sBJgMnukcpl_gz74R4xH9i7A?e=r9KvJj (accessed on 20 July 2024).

For weather station data, Kriging interpolation was performed using the "Smart Map" plugin in QGIS [35] to fill gaps and create continuous spatial representations, which is recognised as an effective multiquadric method for unbiased interpolation [36,37]. Additionally, the Kernel Density Estimator in ArcGIS Spatial Analyst represented the Built Coverage Ratio (BCR) based on spatial concentration.

The integration of various geographical raster and shapefiles resulted in non-uniform spatial properties, thus necessitating a harmonisation process through reprojection and resampling techniques for modelling consistency. This produced a unified geo-package of geo-datasets, thus enabling seamless integration into the analysis. Spatial representations of candidate variables are shown in Figures 4 and 5 as examples (2 out of the 102 raster outputs are part of the geo-dataset).

Table 2. Candidate variables for enhanced modelling of SUHI dynamics.

Category	Variables	Formula	Reference
Land Cover	Normalised Difference Vegetation Index (NDVI)	(NIR-VIS)/(NIR + VIS)	[38–40]
	Proportion Vegetation Index (PVI)	$(NDVI\text{-}NDVI_{min})/(NDVI\text{-}NDVI_{min})$	[38–40]
	Normal Difference Water Index (NDWI)	(GREEN-NIR)/(GREEN + NIR)	[41,42]
	Normal Difference Moisture Index (NDMI)	$(NIR_{short} - SWIR)/(NIR_{short} + SWIR)$	[38,39]
	Albedo	$(\rho NIR + \rho SWIR)/2(1 - \rho RED)$	[43,44]
	Emissivity	(0.004·PVI) + 0.986	[43,44]
	Solar Reflectance Index (SRI)	$[(SR\text{-}SR_{min})/(SR_{max}\text{-}NDVI_{min})] \cdot 100$	[45]
	Land Surface Temperature (LST)	$Tc = (K2/(\ln(K1/L\gamma + 1))) - 273.15$ (*)	[46]
Urban Geomorphology	Buildings and Human Activities	Kernel Density Estimation QGIS tool	[33]
	Normalised Difference Built-Up Index (NDBI)	(SWIR − NIR)/(SWIR + NIR)	[47]
	Sky View Factor (SVF)	SAGA QGIS tool	[34,48]
	Building Coverage Ratio, Building Density	BCR, BD	[14]
	Building Volume and Surface-to-Volume ratio	V, S/V	[14]
Weather Stations	Relative Humidity Wind Speed and Direction Solar Irradiation Air Temperature	Weather stations' measurements (Kriging interpolation in Smart Map QGis tool)	[35–37]

(*) K2, K1, and $L\gamma$ must be retrieved from Landsat 7 and 8 imagery metadata.

Figure 4 present the Kernel analysis of the BCR for Turin in 2001 and 2018. Higher BCR values indicate denser built-up areas. Despite differences in data accuracy from BDTRE cartographies, there is a clear increase in the BCR, especially in peripheral areas.

Figure 5 displays the NDVI, calculated from satellite imagery using NIR and red wavelengths (Table 2). In 2001, Turin's NDVI was near 0, indicating minimal vegetation. By 2018, urban regeneration significantly increased the vegetation, with NDVI values approaching 1.

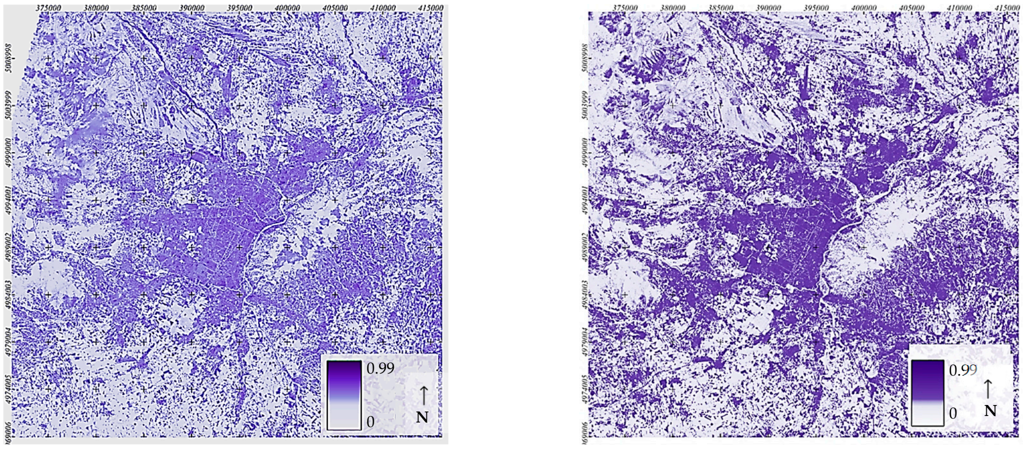

(**a**) (**b**)

Figure 4. Maps of the BCR in Turin (m^2/m^2) in the years (**a**) 2001 and (**b**) 2018. Grid UTM Zone 32N.

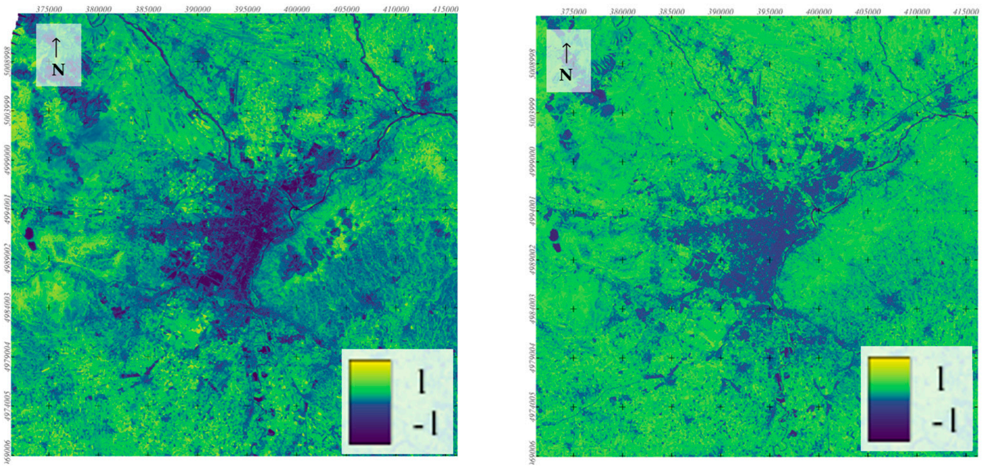

(**a**) (**b**)

Figure 5. Maps of the NDVI in August in the years **(a)** 2001 and **(b)** 2018. Grid UTM Zone 32N.

2.4. Evaluation of the Surface Urban Heat Island Intensity (SUHII)

This study adopted an approach that used the LST to automatically differentiate between urban and suburban areas, thus avoiding reliance on predefined boundaries, as in traditional methods cited in the introduction. SUHII was calculated by normalising the local LST value using the formula [46]

$$SUHII = \frac{LST - LSTmean}{LSTstdev}$$

A positive SUHII indicates a warmer LST than average, thus highlighting intensified urban areas, while a negative SUHII suggests a cooler LST, typically in peripheral regions. This method allowed for context-independent comparisons of variations across different landscapes.

Figure 6 presents the SUHII derived from satellite imagery of Turin and its surroundings. SUHII is more pronounced in areas with high industrial activity, dense buildings, and minimal vegetation (southeast of Turin). In contrast, areas undergoing urban regeneration (northwest), such as the ex-industrial Teksid area, show cooling effects, indicating UHI mitigation in the 2018 image.

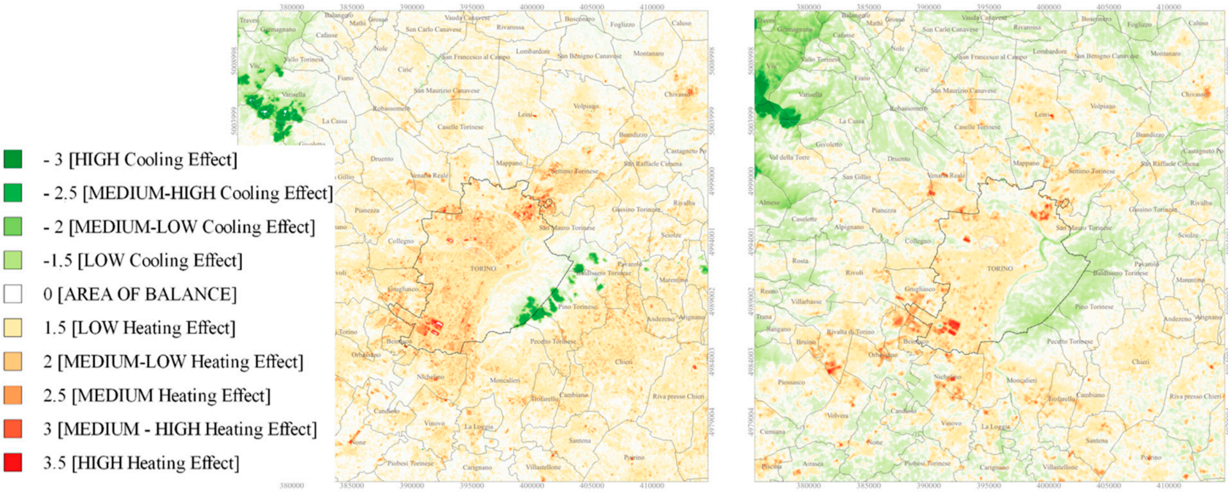

(**a**) (**b**)

Figure 6. SUHII elaborated from satellite imagery in August: (**a**) 2001; (**b**) 2018.

2.5. Correlation Analysis with SUHII

The Pearson correlation coefficient r was used to evaluate the linear relationship between two datasets, such as SUHII and a variable X:

$$r = \frac{\sum(SUHII - SUHII_{avg}) \cdot \sum(X - X_{avg})}{\sqrt{\sum\left(SUHII^2 - {SUHII_{avg}}^2\right)} \cdot \sqrt{\sum\left(X^2 - {X_{avg}}^2\right)}}$$

In this study, r was calculated for a preliminary sensitivity analysis across all 30 m × 30 m cells and census sections in Turin. However, Pearson's coefficient only captures linear relationships, which may not fully represent the complexity of the urban environment. To address nonlinear relationships, a Random Forest model was employed, offering greater flexibility in detecting more complex patterns between SUHII and other variables.

2.6. Machine Learning Modelling: Random Forest Regression

This section presents the model developed to calculate SUHII using a data-driven approach based on the Random Forest (RF) ML algorithm. The RF model was selected due to its ability to manage large datasets and capture complex, non-linear relationships between variables within an urban environment, which is facilitated by the ArcGIS Pro plugin [35]. Prior to integrating the variables into the RF algorithm, hyperparameter tuning was performed using libraries, such as Optuna and Scikit-learn [49]. This process systematically optimised the model's performance by adjusting the hyperparameters (e.g., the variable range, leaf size, and tree depth), thus ensuring that the algorithm operated efficiently.

The geo-package was organised with SUHII as the target variable, while other data and calculated variables served as predictors. The dataset was split into training (80%) and testing (20%) sets. Initially, the RF regression model was trained to learn the relationships between predictor variables and SUHII. The trained model was then validated using the test dataset, with performance assessed through various metrics, such as the Mean Squared Error (MSE), the Root Mean Squared Error (RMSE), and R-squared. To further enhance model accuracy and reliability, a calibration phase was undertaken by adjusting the input parameters and variables. The final model was subsequently used to simulate SUHII across past, present, and future scenarios.

Figure 7 illustrates the operational framework of the model. Beginning with input data organised in a geo-package, the model employs ML algorithms to simulate SUHII by combining variables and iteratively reducing the error between observed and predicted

SUHII values. The RF algorithm generates multiple decision trees, with each using different data combinations. Each tree acts as a decision-making unit by considering certain variables, including the following.

- Leaf size: the minimum number of variables required to stop tree splitting.
- Tree depth: the maximum number of levels a decision tree can reach.

The final prediction is made by averaging the results from all decision trees. A larger number of trees in the forest enhances the accuracy and robustness of the prediction.

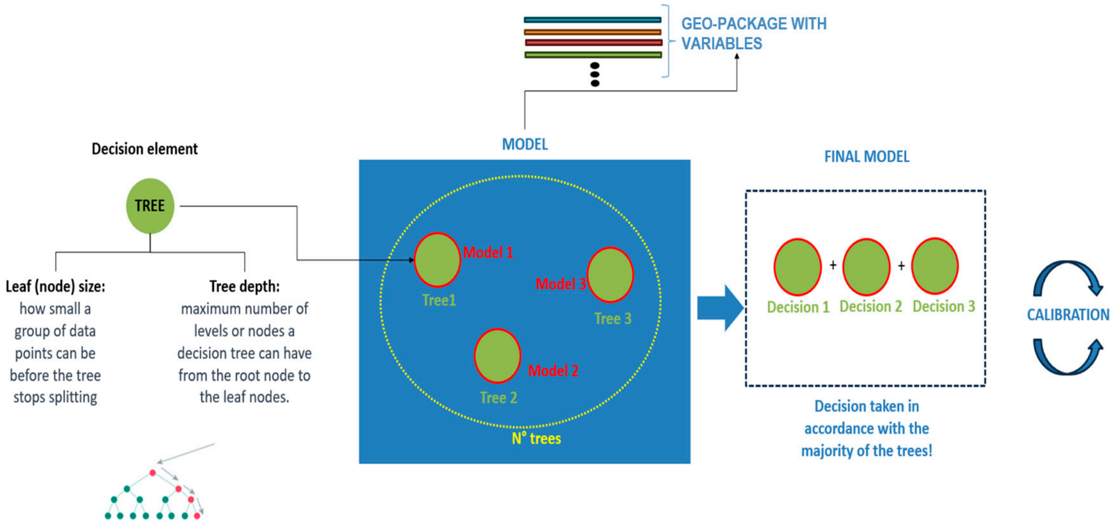

Figure 7. Random Forest regression modelling (authors' own elaboration).

The "Forest-Based Classification and Regression" tool in ArcGIS Pro [49] was used to implement the RF algorithm on a standard personal computer, enabling the creation of training and test datasets and the development of a predictive model for large urban datasets. The model's output was compared with SUHII derived from satellite imagery, and a residual analysis was performed to identify discrepancies.

2.7. The UHI Effects of LCZs and Settlement Morphologies

This section explores the application of the qualitative LCZs method, as defined by Stewart and Oke [9], to the settlement morphologies ("morfologie insediative," m.i.) outlined in the Regional Landscape Plan (RLP) for the City of Turin. The goal was to quantitatively assess the similarities between LCZ and m.i. characteristics in relation to SUHII values.

In the initial phase, LCZ types uncommon in Italian cities, such as LCZ 1 (high-rise business districts) and LCZ 7 (informal settlements), were excluded. Thermal, radiative, and metabolic properties were then assigned to each settlement morphology. These properties were defined as follows:

- Thermal properties, quantified by surface admittance (the ability of a surface to exchange heat, influenced by materials, orientation, moisture, and wind);
- Radiative properties, indicated by surface albedo (the ratio of reflected to incident solar radiation, affected by surface colour, roughness, and moisture);
- Metabolic properties, representing anthropogenic heat output (annual average heat flux from human activities and fuel combustion).

The analysis compared the LCZ and m.i. characteristics with SUHII values, proposing mitigation strategies based on their thermal, radiative, and metabolic properties. The objective was to determine whether the SUHII model, combined with LCZs and m.i., could be used to quantify the effects of mitigation interventions and inform more tailored urban planning strategies.

3. Results

3.1. Linear Correlation Analysis Between SUHII and Urban Variables

Table 3 summarises the results from averaging 1000 SUHII values, effectively minimising the influence of anomalous data. Variables with low correlation, such as heat loss surfaces and building heights, are excluded.

The analysis indicates a positive correlation between SUHII and several variables: the Normalised Difference Built-up Index (NDBI), indicating built-up density; the Normalised Difference Water Index (NDWI), representing water content; building density (BD); and building volume (V).

Conversely, negative correlations are observed with vegetation presence (NDVI), vegetation considering atmospheric variations (PVI), moisture (NDMI), surface emissivity (EM), albedo (ALB), solar reflectance and thermal emission capacity (SRI), and the Sky View Factor (SVF). Correlations for SVF, BD, and V are notably low.

These correlations are specific to the City of Turin and this case study; however, the methodology is applicable to other urban areas.

Table 3. Application field and linear correlation of the average variables with SUHII (for groups of 1000 data; in red negative correlation, in blue positive correlation).

	SUHII	NDVI	PVI	NDBI	EMISSIVITY	ALBEDO	SRI	NDMI	NDWI	SVF	BD	V
minimum	−0.43	−0.09	0.67	−0.41	0.9887	0.08	25.04	0.05	−0.29	0.62	0.03	2839.00
average	1.32	0.05	0.72	−0.18	0.9889	0.12	25.13	0.18	−0.19	0.74	0.19	3800.08
median	1.56	0.01	0.71	−0.14	0.9888	0.11	25.09	0.14	−0.17	0.73	0.20	3575.28
maximum	3.05	0.25	0.79	−0.05	0.9891	0.17	25.27	0.41	−0.09	0.94	0.30	8053.86
Pearson's correlation r		−0.96	−0.95	0.97	−0.95	−0.92	−0.96	−0.97	0.92	−0.47	0.26	0.18

Figure 8 illustrates the relationship between SUHII and the variables listed in Table 4, confirming the direction of the Pearson correlations. The overall trend is well-defined and supported by a high coefficient of determination (R^2). However, exceptions are observed for very low and very high SUHII values, where other variables may influence UHI effects.

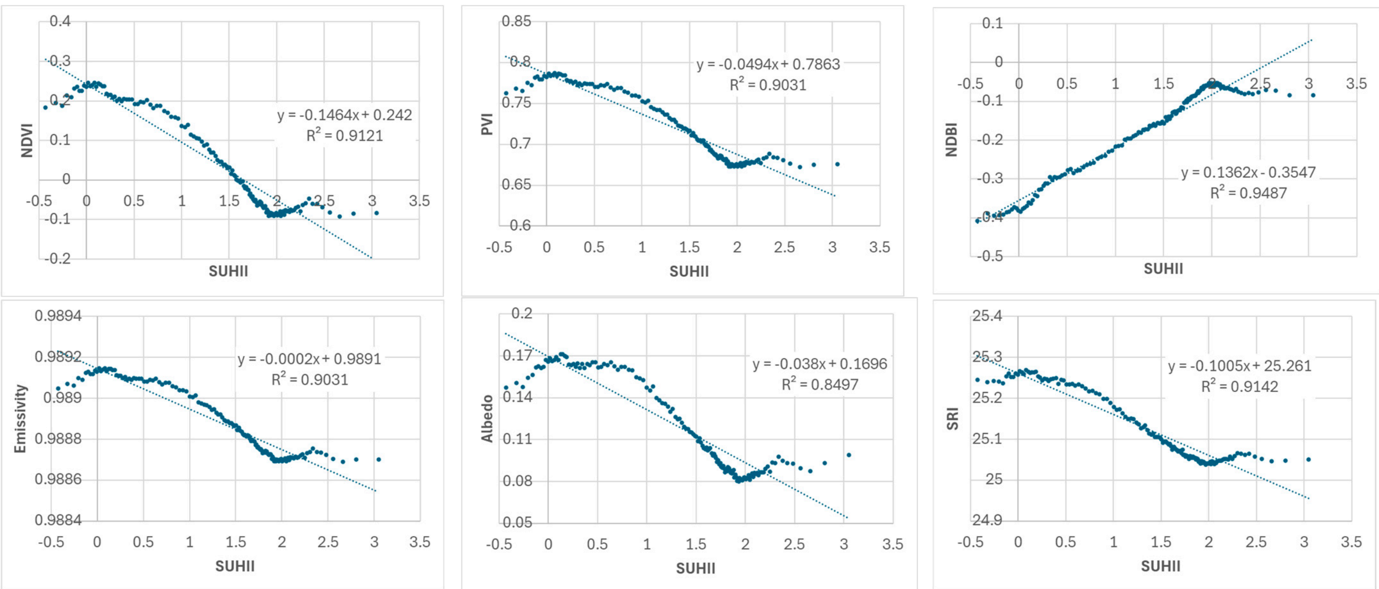

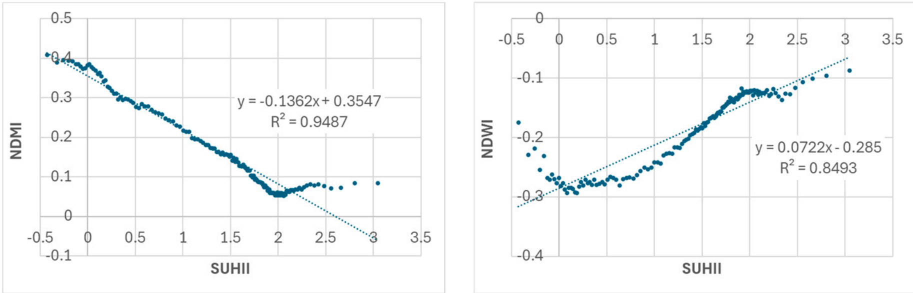

Figure 8. Line fit plots of SUHII-related variables.

Table 4. Parameters used to optimise the performance of RF regression algorithms.

Season	Number of Trees	Number of Randomly Sampled Variables	Leaf Size	Tree Depth Range
Summer 2018	200	5	1	31
Mid-season 2018	59	5	3	13
Winter 2018	60	5	5	25
Summer 2001	59	4	1	39–50
Mid-season 2001	164	4	1	38–44
Winter 2001	97	4	2	16

The independence of the variables was evaluated using multilinear regression. As shown in Figure 9, only the NDVI, NDBI, albedo, and PVI had *p*-values below 0.05. The regression model achieved a high coefficient of determination (R^2 = 0.9872), indicating a strong fit.

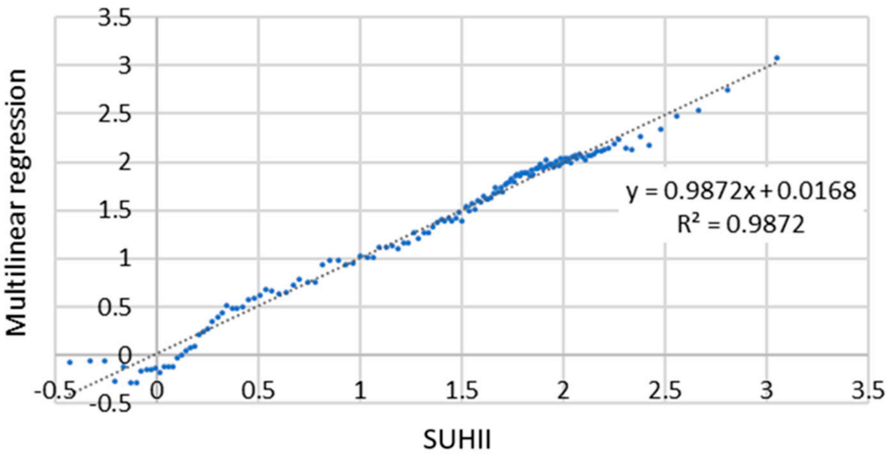

Figure 9. Multilinear regression of SUHII.

3.2. SUHII Modelling with Random Forest Algorithm

The RF algorithm was optimised using the Optuna tool, with the results shown in Table 4. Key hyperparameters—the number of trees, the sampled variables, the leaf size, and the tree depth—were fine-tuned to enhance model accuracy. In 2001, 4 variables were sampled, and in 2018, 5 were sampled, from over 17 in total. The number of trees and the tree depth varied to capture the model's complexity, thus ensuring optimal performance in both training and testing phases.

Table 5 presents the performance of the RF model. MSE and RMSE values, all under 0.08 and 0.283, indicate minimal prediction errors. High R^2 values (0.853 to 0.997) confirm strong model accuracy, while *p*-values < 0.05 demonstrate statistical significance across seasons and years, thus ensuring robust SUHII predictions.

Table 5. MSE, RMSE, R^2, and *p*-value of data-driven model with RF algorithm.

Season	MSE	RMSE	R^2	*p*-Value
Summer 2018	0.023	0.152	0.997	0.001
Winter 2018	0.021	0.145	0.991	0.002
Mid-season 2018	0.080	0.283	0.948	0.001
Summer 2001	0.045	0.212	0.994	0.001
Winter 2000	0.011	0.105	0.853	0.002
Mid-season 2001	0.017	0.130	0.990	0.001

Table 6 shows that the mean residuals are close to zero, indicating accurate predictions by the RF model with minimal systematic error. The low standard deviations across seasons reflect consistent predictive performance.

Table 6. Residuals analysis (mean and standard deviation).

Season	Mean Residuals	Standard Deviation of Residuals
Summer 2018	−0.00041	0.0786
Winter 2018	−0.00020	0.0756
Mid-season 2018	−0.00004	0.2378
Summer 2001	−0.00082	0.1052
Winter 2000	−0.00013	0.0793
Mid-season 2001	−0.00026	0.0682

Table 7 highlights that in 2001, the topography (DTM), built-up areas (NDBI), and Solar Irradiation were the main factors influencing SUHII. By 2018, the built environment gained greater importance, with the BCR (Building Coverage Ratio) the most influential factor, followed by DTM, NDMI, and the Sky View Factor, indicating increasing urbanisation and its effects on SUHII.

Table 7. The weight of variables for the UHII in 2001 and 2018.

2001			2018		
Rank	**Variable**	**Score**	**Rank**	**Variable**	**Score**
1	DTM	6102.32	1	BCR	18023.83
2	NDBI	5555.31	2	DTM	12137.12
3	Solar Irradiation	4327.89	3	NDMI	11733.99
4	NDMI	4197.91	4	Sky View Factor	5901.33
5	Albedo	3251.13	5	NDVI	4767.62
6	Air temperature	2824.21	6	Emissivity	4509.74
7	NDVI	2696.72	7	NDWI	4488.35
8	Emissivity	1950.37	8	Wind speed	4368.62
9	SRI	1801.58	9	S/V Ratio	3173.45
10	Wind direction	1575.72	10	Wind direction	2875.59
11	NDWI	1282.06	11	Relative Humidity	2757.80
12	Wind speed	1090.55	12	Air Temperature	2680.04
13	Air Relative Humidity	1035.66	13	Solar Irradiation	2603.21
14	-	-	14	SRI	2572.03
15	-	-	15	Albedo	2151.66

3.3. Assessing SUHII in the Ex-Industrial Area of Teksid

Analysing SUHII outputs in the Teksid ex-industrial area before and after urban regeneration reveals the effectiveness of the interventions. Figure 10 shows SUHII predictions for different seasons in 2001 and 2018 at the district level generated by the RF model. A marked decrease in SUHII values was observed in 2018, especially during the summer, suggesting that the regeneration efforts had a significant cooling effect.

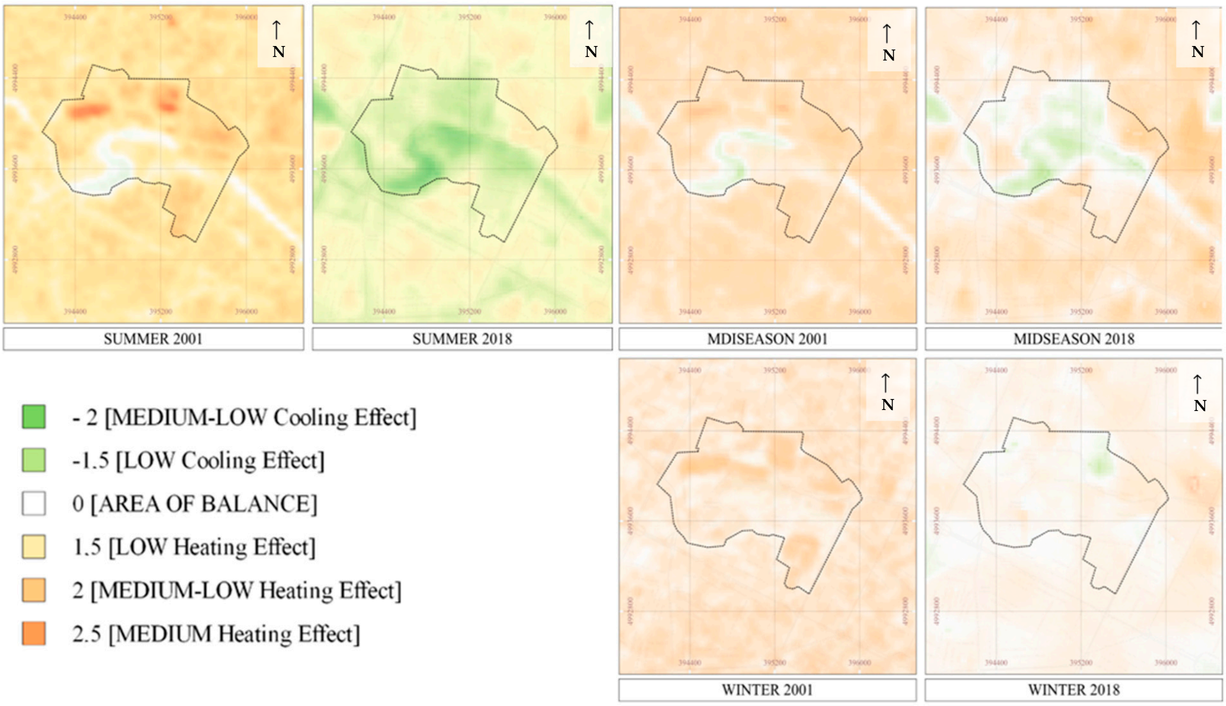

Figure 10. Comparison of SUHII in the different seasons of 2001 and 2018 in the ex-Teksid area.

Table 8 compares SUHII variations between 2001 and 2018 across different scales, showing a substantial reduction in 2018. This decreases, especially during summer (−0.944 SUHII), suggests a strong cooling effect from the interventions. However, the reduction is less pronounced in winter (−0.544, heating systems turned on), reflecting the complexity of UHI dynamics and the need for season-specific mitigation strategies.

Table 8. SUHII variation between 2001 and 2018 in ex-Teksid area, Turin.

Variable	Radius's Distance from Intervention Area [m]	Summer	Spring	Winter	Mean
UHII (ex-Teksid area)	0	−0.944	−1.037	−0.544	−0.841
UHII (district area)	500	−0.413	−0.524	−0.476	−0.471
UHII (Turin's municipal area)	within administrative borders	−0.500	−0.849	−0.492	−0.614

In Table 9, the analysis of percentage changes in key SUHII variables (NDMI, NDVI, and albedo) between 2001 and 2018 highlights the fact that the NDVI notably increased across Turin, particularly in the ex-Teksid area, with rises of +22%, +17%, and +11% in spring, reflecting successful urban regeneration.

The albedo and the NDMI, representing surface properties, also improved citywide, with more pronounced changes during winter. Negative NDMI values in spring indicate lower rainfall in 2018. Overall, these results demonstrate the positive effects of urban interventions on reducing UHIs through enhanced vegetation and surface characteristics.

Table 9. Variation (2001–2018) of key variables contributing to UHIs.

Variable	Scale	Summer	Spring	Winter	Mean
	ex-Teksid	+19.46%	+21.79%	+8.23%	+16.49%
NDVI	district	+6.41%	+16.61%	+7.61%	+10.21%
	Turin	+6.17%	+11.09%	+1.53%	+6.26%
	ex-Teksid	+10.07%	−7.41%	+17.89%	+6.85%
NDMI	district	+6.77%	−4.27%	+17.69%	+6.73%
	Turin	+8.44%	−12.43%	+17.39%	+4.47%
	ex-Teksid	+3.09%	+0.63%	+14.86%	+6.19%
ALBEDO	district	+1.18%	+0.11%	+13.46%	+4.92%
	Turin	+3.72%	+0.23%	+15.40%	+6.30%

Figure 11 illustrates the NDVI map, graphically revealing the increase in vegetation and greenery within the ex-industrial Teksid area in 2018, with the newly established Dora Park prominently located at the centre.

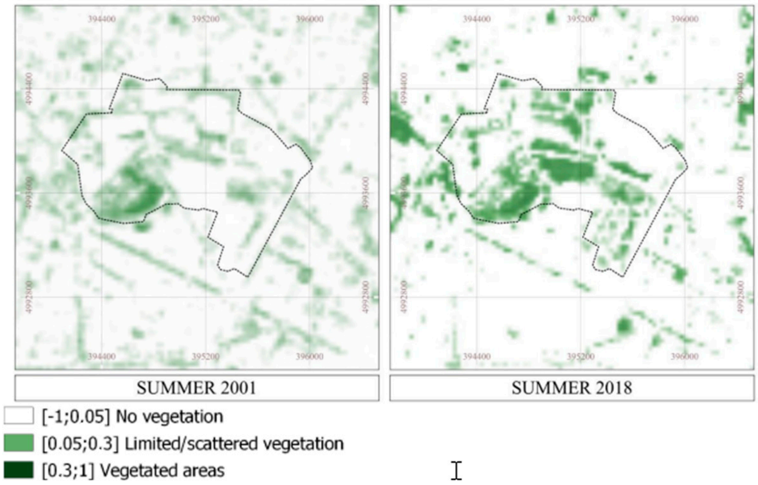

Figure 11. NDVI during summer in 2001 and 2018 in the ex-Teksid area.

In Figure 12, the Dora Riparia River is clearly visible in both years, alongside the new parks established in 2018. Moisture, whether in soil, vegetation, or air, provides a cooling effect that mitigates UHI impacts.

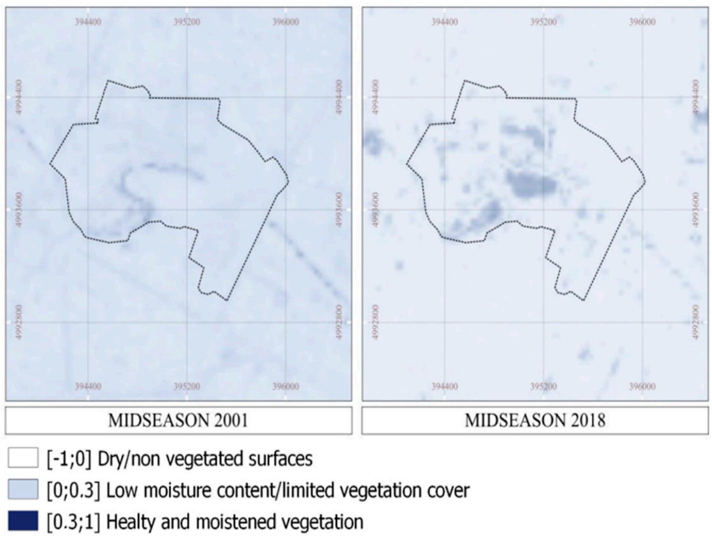

Figure 12. The NDMI during mid-season in 2001 and 2018 in the ex-Teksid area.

Figure 13 shows albedo differences between 2001 and 2018. In 2001, darker colors indicate low reflective areas. By 2018, urban regeneration resulted in increased solar reflectance, represented by lighter colors.

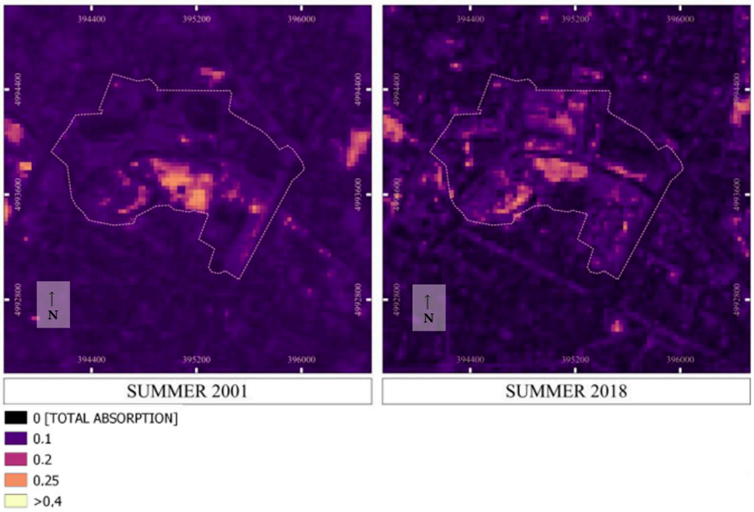

Figure 13. Albedo during summer in 2001 and 2018 in the ex-Teksid area.

Figure 14 indicates a significant decrease in SUHII across the entire municipal territory in 2018. An average decrease of −0.614 was observed when considering all three seasons (summer, winter, and spring/autumn).

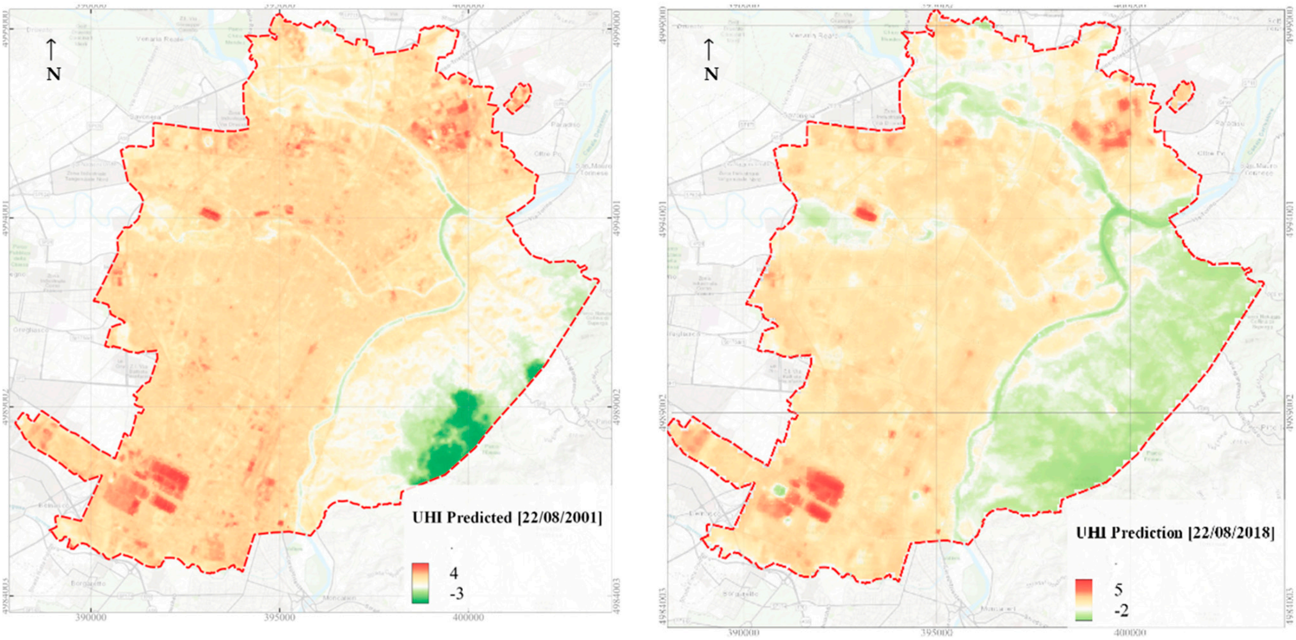

Figure 14. The model of Surface Urban Heat Island Intensity (SUHII) in 2001 and 2018 using the Random Forest regression.

3.4. *The Evaluation of SUHII and Its Mitigation Interventions in Local Climate Zones*

In this section, the UHI effects are compared with the characteristics of the LCZs and typical urban settlements for the City of Turin [50].

Table 10 provides average values for surface admittance, albedo, and anthropogenic heat output for the City of Turin [9]. The LCZs consider typical urban areas with low-rise (1–3 stories, height < 9 m), mid-rise (4–9 stories, height 9–24 m), and high-rise (10+ stories, height > 24 m) buildings. The albedo of asphalt surfaces typically ranges from 0.15 to 0.30, although studies in Italy report values between 0.05 and 0.20 [51]; as such, a value of 0.10 was considered [52]. For asphalt surfaces, such as those at airports and on roads, a value of 0.10 was used, while mining and extractive areas were assigned a value of 0.225.

Some LCZs are not present in the urban area of the City of Turin, and they were neglected in this study (in grey).

Table 10. Average values of surface admittance, albedo, and anthropogenic heat output; in grey are the LCZs not identified in the Metropolitan City of Turin.

Local Climate Zone	Surface Admittance ($J\ m^{-2}\ s^{-1/2}\ K^{-1}$)		*Average*	Surface Albedo (-)		*Average*	Anthropogenic Heat Output ($W\ m^{-2}$)	
LCZ 1 compact high-rise	*1500*	*1800*		*0.10*	*0.20*		*50*	*300*
LCZ2 compact mid-rise area	1500	2000	*1850*	0.10	0.20	*0.15*	>75	
LCZ 3 compact low-rise	1200	1800	*1500*	0.10	0.20	*0.15*	>75	
LCZ 4 open high-rise area	1400	1800	*1600*	0.12	0.25	*0.185*	>50	
LCZ 5 open mid-rise area	1400	2000	*1700*	0.12	0.25	*0.185*	>25	
LCZ 6 open low-rise area	1200	1800	*1500*	0.12	0.25	*0.185*	>25	
LCZ 7 lightweight low-rise	*800*	*1500*		*0.15*	*0.35*		*>35*	
LCZ 8 large low-rise area	1200	1800	*1500*	0.15	0.25	*0.20*	>50	
LCZ 9 sparsely built area	1000	1800	*1400*	0.12	0.25	*0.185*	>10	
LCZ 10 heavy industry	1000	2500	*1750*	0.12	0.20	*0.16*	>300	
LCZ A dense trees	*unknown*			*0.10*	*0.20*		*0*	
LCZ B scattered trees	1000	1800	*1400*	0.15	0.25	*0.20*	0	
LCZ C bush, scrub	*700*	*1500*		*0.15*	*0.30*		*0*	
LCZ D low plants	1200	1600	*1400*	0.15	0.25	*0.20*	0	
LCZ E bare rock or paved	1200	2500	*1850*	0.15	0.30	*0.10 */0.225*	0	
LCZ F bare soil or sand	*600*	*1400*		*0.20*	*0.35*		*0*	
LCZ G water	*1500*			*0.02*	*0.10*		*0*	

* Typical value for asphalt pavements in Italy.

Table 11 joins the characteristics of the LCZs with the settlements' morphologies m.i. from the Regional Landscape Plan (RLP) of Piedmont Region.

Table 11. Association between the settlements' morphologies ("m.i." in Italian) and the LCZs.

Association of Settlement Morphologies with Local Climate Zones	
Settlements' Morphologies by RLP ("Morfologie Insediative m.i." in Italian)	**Local Climate Zone (LCZ)**
(m.i. 1)—Consolidated urban areas of major centres	LCZ 2—Compact mid-rise area
(m.i. 2)—Consolidated urban areas of minor centres	LCZ 3—Compact low-rise area
(m.i. 3)—Urban fabrics outside of urban centres	LCZ 4—Open high-rise area
(m.i. 4)—Discontinuous suburban fabrics	LCZ 5—Open mid-rise area
(m.i. 5)—Organised specialised settlements	LCZ 10—Heavy industry
(m.i. 6)—Dispersed areas, mainly residential	LC6—Open low-rise area
(m.i. 7)—Dispersed areas, mainly specialised	LC8—Large low-rise area
(m.i. 8)—Specialised islands	LCZ E—Bare rock or paved
(m.i. 9)—Infrastructural complexes	LCZ E—Bare rock or paved
(m.i. 10)—Rural areas in plains or hills	LCZ 9—Sparsely built area
(m.i. 11)—Systems of rural nuclei in plains, hills, low mountains	LCZ 9—Sparsely built area
(m.i. 12)—Mountain villages	LCZ B—Scattered trees + LCZ 9—sparsely built area

(m.i. 13)—Rural areas in mountains or hills with scattered and dispersed buildings	LCZ B—Scattered trees + LCZ 9—sparsely built area
(m.i. 14)—Rural areas in plains	LCZ D—Low plants
(m.i. 15)—Mountain pasturelands and high-altitude rural settlements	LCZ D—Low plants + LCZ 9—sparsely built area

Table 12 summarises the average characteristics of surface admittance, surface albedo, and anthropogenic heat output for different m.i.s. Specific land uses—including large commercial structures, hospitals, prison areas, logistics hubs, motorway infrastructures, sports facilities, and cemeteries—exhibited distinct characteristics associated with various LCZs.

Table 12. Association between settlement morphologies and the characteristics of LCZs.

Note	**Association of LCZ and m.i. by RLP**		***Surface Admittance***	***Surface Albedo***	***Anthropogenic Heat Output***
			(J m^{-2} $s^{-1/2}$ K^{-1})	**(-)**	**(W m^{-2})**
	m.i. 1	LCZ 2	1850	0.15	75
	m.i. 2	LCZ 3	1500	0.15	75
	m.i. 3	LCZ 4	1600	0.185	50
	m.i. 4	LCZ 5	1700	0.185	25
* With refineries **(former m.i. 8)**	m.i. 5 *	LCZ 10	1750	0.16	300
	m.i. 6	LCZ 6	1500	0.185	25
* With large commercial structures, purification plants, hospitals, military and prison areas (**former m.i. 8),** warehouses, rail junctions, logistics hubs, and nodes **(former m.i. 9)**	m.i. 7 *	LCZ 8	1500	0.20	50
* Contains only mining areas/extraction plants	m.i. 8 *	LCZ E	1850	0.225	0
* Contains runways (albedo value variation *)	m.i. 8 *	LCZ E *	1850	0.10 *	0
* With energy production systems (e.g., photovoltaic systems)	m.i. 9 *	LCZ E	1850	0.225	0
* With motorway infrastructures (change in albedo value *)	m.i. 9 *	LCZ E *	1850	0.10 *	0
* With theme parks, campsites, sports facilities, golf clubs, cemeteries **(former m.i. 8)**	m.i. 10 *	LCZ 9	1400	0.185	10
	m.i. 11	LCZ 9	1400	0.185	10
	m.i. 12	LCZ B + LCZ 9	1400	0.1925	10
	m.i. 13	LCZ B + LCZ 9	1400	0.1925	10
	m.i. 14	LCZ D	1400	0.20	0
	m.i. 15	LCZ D + LCZ9	1400	0.1925	10

* For some specific categories of m.i.s, the associations with LCZs were re-defined, as indicated in the column Note.

Figure 15 shows that for the urban area, it is possible to distinguish the LCZ 2 (compact mid-rise), the LCZ 3 (compact low-rise), and the LCZ 4 (open high-rise); in the suburbs, it is possible to distinguish the LCZ 9 (sparsely built), the LCZ 10 (heavy industry), and the LCZ E (bare rock or paved).

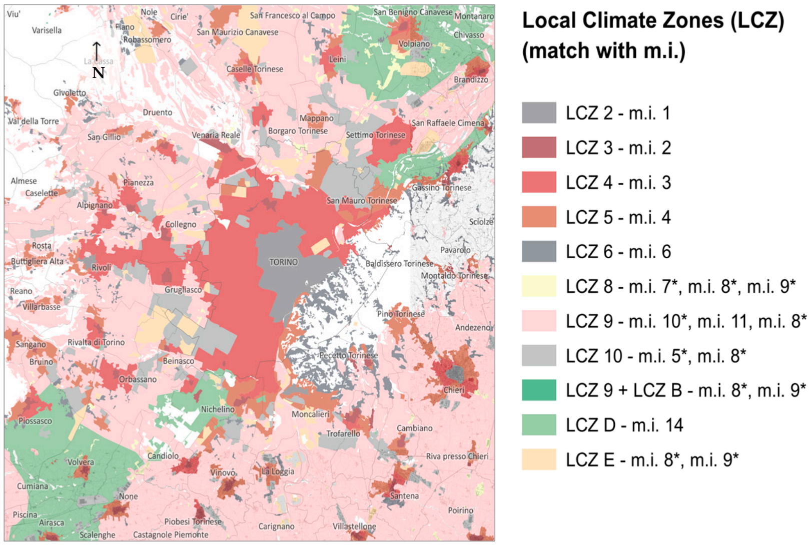

Figure 15. Cartographic representation of LCZs' and urban settlements' m.i.s for the city of Turin and its surroundings (as specified in Table 12).

Figure 16 compares anthropogenic heat output from LCZs with SUHII values for August 2021, revealing clear correspondences. These are particularly evident in productive areas, such as the industrial zone in the southwest of Turin (light-green circles), the northeast (yellow circle), and the Teksid area (light-blue circle).

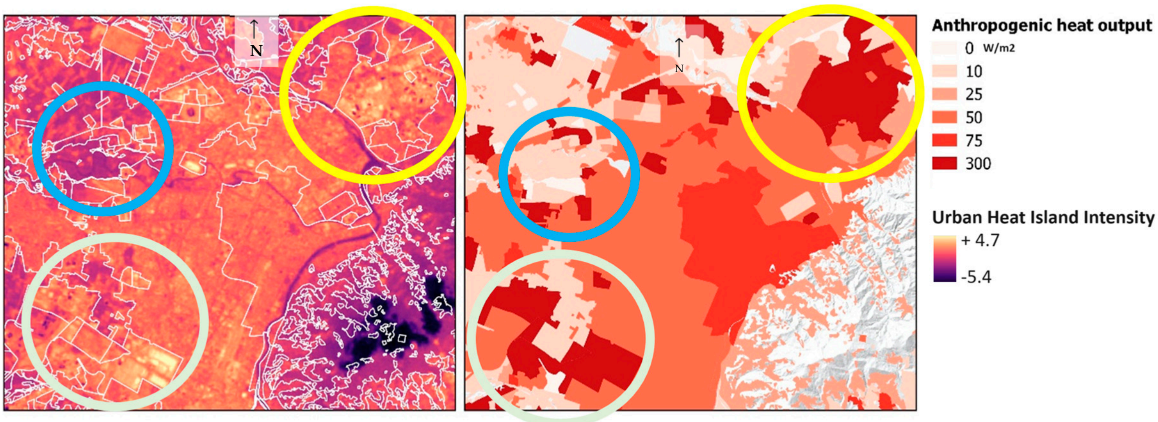

Figure 16. Comparison between the results of the SUHII model in August 2021 (on the left) and the anthropogenic heat output of Local Climate Zones (on the right).

Settlement morphologies requiring priority for UHI mitigation were identified based on thermal, radiative, and metabolic properties. The SUHII analysis in Figure 16 shows the highest surface admittance in consolidated urban fabrics (m.i. 1), specialised islands (m.i. 8), infrastructure complexes (m.i. 9), and areas outside of the urban centre (m.i. 4). Lower albedo values were found in specialised islands (m.i. 8), infrastructure complexes (m.i. 9), and consolidated fabrics (m.i. 1, m.i. 2). The highest anthropogenic heat output was recorded in organised specialised settlements (m.i. 5).

Table 13 establishes a priority order for UHI mitigation, aiding energy governance at both urban and building scales.

Table 13. Settlement morphologies with worse thermal, radiative, and metabolic properties (in a priority order for UHI-mitigation interventions).

Priority Order	Thermal Properties	Radiative Properties	Metabolic Properties
1	Consolidated urban areas of major centres **(m.i. 1)**	Specialised islands **(m.i. 8) ***	Organised specialised settlements **(m.i. 5)**
2	Specialised islands **(m.i. 8) ***	Infrastructural complexes **(m.i. 9) ***	Consolidated urban areas of major and minor centres **(m.i. 1, m.i. 2)**
3	Infrastructural complexes **(m.i. 9) ***	Consolidated urban areas of major and minor centres **(m.i. 1, m.i. 2)**	Urban fabrics outside of centres **(m.i. 3)**
4	Organised specialised settlements **(m.i. 5) ***	Organised specialised settlements **(m.i. 5) ***	Dispersed areas, mainly specialised **(m.i. 7)**
5	Discontinuous suburban fabrics **(m.i. 4)**		

The type of intervention to mitigate an UHI, however, greatly depends on the type of territorial context. The LCZ approach recommends targeting thermal, radiative, and metabolic properties and tailoring strategies to specific settlement morphologies. Table 14 outlines some of these interventions.

Table 14. Interventions to mitigate the UHI based on improving thermal, radiative, and metabolic properties of settlement morphologies.

Properties (To Improve)	Settlement Morphologies	Types of Interventions
Thermal properties	Consolidated urban areas of major centres **(m.i.1)** Specialised islands **(m.i. 8) *** Infrastructural complexes **(m.i. 9) *** Organised specialised settlements **(m.i.5) *** Discontinuous suburban fabrics **(m.i. 4)**	• **Use of cool materials** with a high Solar Reflectance Index (SRI) for roofs and pavements; they provide cooler surfaces by combining a high albedo with a high thermal emissivity in the infrared spectrum. • **Green roofs**, or rooftop gardens, which provide shadows and reduce the temperatures of roofs and the surrounding air. • **Planting trees and increasing vegetation coverage**. Trees and vegetation lower surface and air temperatures through shading and evapotranspiration; shaded surfaces can be cooler by 11–25 °C compared to peak temperatures of unshaded materials; evapotranspiration, alone or in combination with shading, can help reduce peak summer temperatures by 1–5 °C (EPA - US). • **Urban cooling systems**, like water parks, fountains, or evaporative surfaces, contribute to cooling the surrounding environment. • **Use of permeable materials** that allow water to infiltrate the soil and contribute to cooling through evapotranspiration and more water content; they also drain excess water during heavy rainfall events, known as "water bombs". • **Promote passive cooling strategies** that reduce energy use inside of buildings (e.g., natural ventilation, evaporative cooling, geothermal cooling). • **Adopt building and urban certification systems** that ensure minimal and optimal use of energy considering the climatic conditions and the best technologies on the market in accordance with environmental protocols in order to achieve higher certification scores (ITACA Urban scale certification, GBC Historic Building Protocol, LEED® Protocol).
Radiative properties	Specialised islands **(m.i. 8) *** Infrastructural complexes **(m.i.9) *** Consolidated urban areas of major and minor centres **(mm.ii. 1, 2)**	• **High solar reflectance or albedo materials** for the external surfaces of buildings, such as roofs, walls, and pavements, with high albedo combined with a high thermal emissivity in the infrared spectrum. • **Adopting building and urban certification systems** that ensure minimal and optimal use of energy considering the climatic conditions and the best technologies on the market in accordance with environmental protocols in order to achieve higher certification scores (ITACA Urban scale certification, GBC Historic Building Protocol, LEED® Protocol).

	Organised specialised settlements **(m.i. 5) ***	
Metabolic properties	Organised specialised settlements **(m.i. 5)** Consolidated urban areas of major and minor centres **(m.i. 1, m.i. 2)** Urban fabrics outside of centres **(m.i. 3)** Areas of predominantly specialised dispersion **(m.i. 7)**	• **Provide dedicated roads** (non-communal lanes) for public urban transportation in order to make the service more convenient compared to private vehicles. • **Ensure the continuity of urban cycling paths** by planning a functional system that facilitates systematic travel from home to work and from home to school. • **Implement specific regulatory provisions** for urban development instruments as well as building regulations (also for productive settlements) with the aim of employing bioclimatic construction technologies, eco-tech, and climate-proof materials. • **Research and use the Best Available Technologies (BATs)**, especially for industrial processes. • **Implement specific energy efficiency measures** (building retrofit measures, replacement of public lighting sources and fixtures, regulation and control systems for District Heating Network, etc.). • **Utilise renewable energy sources** (e.g., photovoltaic installations on rooftops, geothermal energy, sharing energy with Renewable Energy Communities—RECs). • **Adopt building and urban certification** systems that ensure minimal and optimal use of energy considering the climatic conditions and the best technologies on the market in accordance with environmental protocols to achieve higher certification scores (ITACA Urban scale certification, GBC Historic Building Protocol, LEED® Protocol).

4. Discussion

This study offers valuable insights into Urban Heat Island mitigation in the Metropolitan City of Turin by combining Random Forest modelling with LCZs. This integrated approach enables the identification of targeted mitigation strategies tailored to the unique morphological and environmental characteristics of urban areas, thus providing a more precise solution than previous UHI studies that analysed approaches individually. Our integrated methodology aims to quantitatively demonstrate, through a case study analysis, the effects of mitigation interventions following urban regeneration on UHIs.

Many prior studies have emphasised generalised interventions, such as enhancing green infrastructure or improving albedo, but they often limited their considerations to correlations without adequately addressing local urban morphologies and their interrelations.

Our findings suggest that mitigation strategies should vary across different land-use types and settlement forms, highlighting the significance of thermal, radiative, and metabolic properties. For instance, compensatory measures in consolidated urban fabric, where bioclimatic urban planning and UHI mitigation strategies can only be partially applied, present a recurring challenge for UHI management. This research demonstrates that dense urban areas, which are more vulnerable to heat islands, can benefit from alternative strategies, such as improving surface reflectivity (albedo) and incorporating water-based cooling systems.

As observed in the Teksid area, where several mitigation interventions have been applied—including increasing greenery, improving reflectivity, and enhancing humidity with vegetation—this study advances prior work by providing a method to quantify the effectiveness of these interventions through RF modelling to evaluate their impact across diverse urban zones.

Furthermore, by emphasising the need for integrated, adaptive strategies and community involvement, this research contributes significantly to the fields of urban planning and climate resilience, thus providing actionable insights for future urban development. By connecting UHI mitigation with frameworks like the “Mayors Pact” and regional initiatives, such as PEARs, this research situates UHI interventions within a broader context of climate adaptation and resilience.

However, these findings are place-based and may not be generalisable to other urban contexts with different climatic or cultural conditions. Additionally, reliance on detailed urban morphological data for LCZ classification may limit applicability in cities lacking such data. Future research should explore the adaptability of this approach in diverse urban environments by incorporating projected climate change impacts for a more comprehensive understanding of UHI mitigation strategies.

5. Conclusions

This research significantly facilitates the understanding of the UHI phenomenon in the Metropolitan City of Turin by employing an innovative methodology that integrates Random Forest (RF) modelling with LCZs. The analysis revealed a substantial reduction in the SUHII of −0.94 in summer and −0.54 in winter in the Teksid area, which is attributable to targeted urban mitigation interventions, such as increased vegetation (higher NDVI), higher albedo, and reduced impervious surfaces (lower Built Coverage Ratio). These results quantitatively demonstrate the effectiveness of urban regeneration efforts in mitigating UHI effects in a historically industrial context.

These findings underline the critical role of environmental factors, including albedo and surface emissivity, in shaping urban thermal profiles. The integration of quantitative and qualitative analyses allowed for the identification of tailored mitigation strategies that align with the unique morphological characteristics of different urban areas.

The key findings are the following.

- Effective Mitigation Strategies: This study highlights those specific interventions, such as enhancing green infrastructure and improving surface reflectivity, that can significantly reduce UHI intensity in dense urban areas. Almost 1 point of the SUHII decreased in the Teksid area after mitigation.
- Methodological Innovation: By combining machine learning with geospatial data, this research establishes a robust framework for future studies on UHIs, thus allowing for precise modelling and assessment of mitigation strategies across diverse urban landscapes. GIS, ML, and LCZs are included in a single methodology.
- Policy Recommendations: The results advocate for a shift in urban planning practices towards a more integrated, place-based approach that incorporates climate considerations across various sectors, thus promoting coordinated actions that address UHIs.

The methodology can be replicated in other urban contexts by utilising freely available GIS and satellite data to create localised UHI models. By fostering community engagement and collaboration among stakeholders, this research provides a roadmap for cities to implement effective, adaptive strategies for a climate-resilient future.

Author Contributions: Conceptualisation, G.M.; methodology, G.M., A.S., X.S., and S.G.; software, A.S. and X.S.; investigation, G.M., A.S., X.S., and S.G.; data curation, A.S., X.S., and S.G.; writing—original draft preparation, G.M., A.S., X.S., and S.G.; writing—review and editing, G.M., A.S., X.S., and S.G.; supervision, G.M. All authors have read and agreed to the published version of the manuscript.

Funding: This research received no external funding.

Institutional Review Board Statement: Not applicable.

Informed Consent Statement: Not applicable.

Data Availability Statement: The data from this study are not publicly available due to privacy and specific agreements.

Acknowledgments: The authors are grateful to Ahad Montazeri for helping with machine learning modelling and to the "Master di II Livello Metodi e Tecniche per il Governo di Territori Resilienti. Verso la gestione integrata dei rischi" of Politecnico di Torino, which have inspired this research regarding the impact of territorial planning on mitigating the urban heat island.

Conflicts of Interest: Authors Alessandro Scalise and Xhoana Sufa were employed by the company Planet Smart City. The remaining authors declare that the research was conducted in the absence of any commercial or financial relationships that could be construed as a potential conflict of interest.

Nomenclature

BCR	Building Coverage Ratio
DTM	Digital Terrain Model
GIS	Geographic Information System
LCZ	Local Climate Zone
LST	Land Surface Temperature
m.i.	Settlements' morphologies ("morfologie insediative" in Italian)
MSE	Mean Squared Error
NDBI	Normalised Difference Built-Up Index
NDMI	Normalised Difference Moisture Index
NDVI	Normalised Difference Vegetation Index
NDWI	Normalised Difference Water Index
NIR	Near InfraRed
PVI	Proportion Vegetation Index
QGIS	Quantum GIS
R^2	Coefficient of determination
RF	Random Forest
RMSE	Root Mean Squared Error
S/V	Surface-to-Volume ratio of buildings
SRI	Solar Reflectance Index
SUHII	Surface Urban Heat Island Intensity
SVF	Sky View Factor
SWIR	Short-wave Infrared
UHI	Urban Heat Island
UHII	Urban Heat Island Intensity
V	Building volume
VIS	Visible

Appendix A

N°	Year	Place	Scale	Object	Factors	Methodology	Results	Keyword
3	1833	LDN	Urban	Analysis and characterisation of the climate of London.	Atmospheric conditions.	Systematic observations of factors at regular intervals throughout the day to assess long-term climate trends in the city.	Howard provided a comprehensive understanding of London's climate and detailing factors.	Investigation
4	1976	VAN	Urban	Causes of the UHI: Canopy and Boundary Layers.	Surface properties, land use, and atmospheric conditions.	Differentiate spatial heat island patterns within Urban Canopy and Boundary Layers.	The study found a clear differentiation between Canopy and Boundary Layer UHIs, influenced by various factors.	Investigation
5	1982	VAN	Urban	Investigating the physical processes driving the UHI effect.	Surface cover, building materials, anthropogenic heat, weather conditions, urban morphology.	Comparing energy fluxes between urban and rural areas quantifies the UHI's effect on temperature disparities.	Urban areas have higher night-time temperatures than rural areas, highlighting the importance of urban energy balance.	Investigation

9	2017	BRA	Urban	Develop and validate a GIS-based extension model capable of accurately calculating UHII.	Urban geometry and meteorological data.	They collected urban geometry and meteorological data, applied a mathematical model to estimate the UHII, and validated it using empirical data in MATLAB.	The outcome is a computational tool named THIS enabling simulation of hypothetical urban scenarios and assessment of the impact of urban geometry.	GIS
10	2018	SZ	Urban	Ventilation corridor planning to mitigate UHIs.	Built environment, wind patterns, land use distribution.	GIS-based case study to analyse wind environments by mapping urban features, assessing wind patterns, and pinpointing suitable corridors for natural ventilation.	Recommendations for urban planning in Shenzhen to improve air quality and comfort through strategic development of natural ventilation corridors.	GIS
11	2018	HK	Local	The study mapped the spatial distribution of nocturnal UHIs using the Local Climate Zone framework.	Climate data and urban morphology data (total street length, pervious surface fraction, Sky View Factor).	GIS, GPS, and Landsat 8 images were used alongside Multiple Linear Regression (MLR) and Partial Least Squares Regression (PLSR) to analyse the spatial distribution of nocturnal UHIs.	Identification of UHI hotspots through the statistical models, with the statement that urban forms have significant influences on UHI development.	GIS
12	2019	HIJ	Urban	Develop and implement a GIS-based model for mitigating the UHI effect in Hiroshima.	Urban morphology, vegetation, density of population, surface types.	GIS to analyse various urban parameters affecting heat absorption and retention. They collected data to create spatial models for predicting heat distribution across the city.	Study of the effectiveness of different mitigation strategies, such as green infrastructure and urban planning interventions, in reducing urban heat.	GIS
13	2021	TRN	Urban	Smart rooftops.	Roof suitability, context, codes, regulations.	Data analysis techniques (GIS), design strategies, and implementation frameworks to optimise the use of urban rooftops for sustainability.	A method to assess rooftop renovation opportunities by evaluating energy savings, thermal comfort, and environmental/economic benefits was introduced.	GIS
14	2022	TRN	Urban	Outdoor thermal conditions at the urban scale.	Urban morphology, vegetation, outdoor thermal comfort, Sky View Factor, mean radiant	Utilised geospatial assessment QGIS [UMEP-SOLWEIG (QGIS)], DSM, and field measurements to evaluate outdoor	SOLWEIG is a more suitable tool for assessment and analyses at the urban scale, while ENVI-met is more useful for feasibility studies	GIS

					temperature, urban surfaces.	thermal comfort on an urban scale.	with high spatial and temporal resolution or for the pre-design phase of little neighbourhoods.	
15	2013	XIA	Regional	Landsat 8 imagery for considering factors like climate, soil, vegetation, and acquisition timing.	Pervious and impervious surface, LST.	They conducted remote sensing analysis to grasp how impervious surface expansion affects local Land Surface Temperature dynamics in the subtropical city.	Growing impervious surfaces had increased Land Surface Temperatures, showing urbanisation's impact on subtropical city temperatures.	Remote sensing
16	2019	USA	Regional	UHI phenomenon in 54 US cities over 15 years, examining its correlation with temperature changes, weather conditions, and urban warming trends.	UHI, temperature variation, climate zones, weather conditions, urban warming trends.	They analysed UHI intensity across cities using satellite data under different temperature conditions. Statistical methods were used to evaluate changes in the UHII concerning temperature variations.	In 38 out of 54 US cities, UHI intensity decreases as temperatures rise, regardless of the climate zone. This is propelled by rural area changes, particularly during moist weather, without a significant UHI effect increase in warming cities.	Remote sensing
17	2021	LX	Regional	Local weather types of data based on Copernicus Land Monitoring Service climate variables dataset.	Thermal patterns (seasons); hourly air temperature, specific humidity, relative humidity, and wind speed data.	Likely involved collecting and processing Lisbon's temperature and weather data, categorising local weather types, and correlating them with UHI intensity variations across the metropolitan area.	UHI intensity estimated in an R script using various factors.	Remote sensing
18	2022	CN	Urban	Ventilation corridor planning to mitigate UHIs.	LST, atmospheric data.	A systematic approach combining data collection (satellite images), quantitative analysis, and validation to effectively identify urban ventilation corridors.	Seven primary ventilation corridors primarily consisted of water bodies and green land areas, while four secondary ventilation corridors were mainly composed of roads.	Remote sensing
19	2022	SZ	Urban	Relationship between the morphological spatial pattern of green space and UHI intensity using	Urban morphology, land cover, morphological characteristics of green spaces, population, buildings.	Employed machine learning methods to analyse the connection between the spatial arrangement of green spaces and the UHI effect.	The UHI intensity was negatively correlated with the cores, perforations, and loops of green space but positively correlated with islets.	Machine learning

				machine learning methods.				
20	2021	NAP	Urban	Predicting nocturnal SUHI at night; use of Random Forest approach to predict LST.	LCZ, land cover, air temperature, LST, short-wave and long-wave radiation, albedo, DEM.	Random Forest in R was used to analyse Landsat 8 and MSG-SEVIRI data in QGIS, and they used the NASA atmospheric calculator and GRASS-GIS to predict Naples's heatwave nocturnal UHIs.	An energy-balance-based machine learning approach to describe the daily cycle of the heat flux components and to predict the nocturnal LST and SUH during an HW event.	Machine learning
21	2021	WH	Urban	Machine learning to simulate and mitigate extreme UHI effects in a factory area.	Industrial morphology, type, production stage, scale, and internal structure.	Satellite data (Landsat 8) and ground measurements were processed with ENVI and MATLAB to apply ML for simulating and mitigating extreme UHI effects in a factory area.	The results show that the scale of all types of factories affects the LST.	Machine learning
22	2022	MAD	Urban	Modelling SHUI through ArcGIS plugin; predict observed LST with high accuracy using Random Forest regression (RFR).	Building height, albedo, DTM, land cover map, LST.	ArcUHI automates UHI modelling using GIS and machine learning, involving data pre-processing, feature selection, model training, validation, and mapping UHI patterns in urban areas.	Development of an add-in (ArcUHI) for automated modelling of the UHI effect.	Machine learning
23	2022	AMD	Urban	Employed a machine learning algorithm to predict factors.	LULC maps, BI, NDVI, NDBI, NDMI, MNDWI.	Satellite imagery and ground-based measurements to train the algorithm by incorporating factors to characterise the surface UHI phenomena.	More than 70% of the area in summer and 40% in winter would likely face higher temperature zones than their respective present situations.	Machine learning
24	2023	AU	National	ML models to assess the link between health outcomes, heat, and air quality exposure in diverse Australian urban areas.	Census, health, land use, point of interest, Google Earth engine, LST.	Investigate the correlation between health metrics and exposure to heat and air quality in various urban areas across Australia.	Social and built environmental factors are more influential on physical and mental health outcomes than heat and air pollution, especially in rural areas.	Machine learning

References

1. United Nations Environment Programme (UNEP). UN Launches Challenge for Cities to Harness Power of Nature for Cooling. Available online: https://www.unep.org/news-and-stories/press-release/un-launches-challenge-cities-harness-power-nature-cooling (accessed on 5 January 2024).

2. United Nations Conference on Trade and Development (UNCTAD) Handbook of Statistics 2023. Available online: https://unctad.org/publication/handbook-statistics-2023 https://www.un-ilibrary.org/content/periodicals/22253270 (accessed on 20 July 2024).
3. United Nations Conference on Trade and Development (UNCTAD). Total and Urban Population. Available online: https://hbs.unctad.org/total-and-urban-population/ (accessed on 5 January 2024).
4. Howard, L. *The Climate of London*; Harvey and Darton: London, UK, 1833.
5. Oke, T.R. The distinction between canopy and boundary-layer urban heat islands. *Atmosphere* **1976**, *14*, 268–277. https://doi.org/10.1080/00046973.1976.9648422.
6. Voogt, J.A.; Oke, T.R. Thermal remote sensing of urban climates. *Remote Sens. Environ.* **2003**, *86*, 370–384. https://doi.org/10.1016/S0034-4257(03)00079-8.
7. Oke, T.R. The energetic basis of the urban heat island. *Q. J. R. Meteorol. Soc.* **1982**, *108*, 1–24.
8. Oke, T.R. *Boundary Layer Climates*, 2nd ed.; Routledge: Methuen, MA, USA, 1987
9. Stewart, I.D.; Oke, T.R. Local climate zones for urban temperature studies. *Bull. Am. Meteorol. Soc.* **2012**, *93*, 1879–1900.
10. Nakata-Osaki, C.M.; Souza, L.C.L.; Rodrigues, D.S. Tool for Heat Island Simulation: A GIS extension model to calculate urban heat island intensity based on urban geometry. *Comput. Environ. Urban Syst.* **2017**, *64*, 297–308. https://doi.org/10.1016/j.compenvurbsys.2017.04.002.
11. Liu, X.; Huang, B.; Li, R.; Zhang, J.; Gou, Q.; Zhou, T.; Huang, Z. Wind environment assessment and planning of urban natural ventilation corridors using GIS: Shenzhen as a case study. *Build. Environ.* **2018**, *129*, 100–113.
12. Liao, K.; Hong, Y.; Heo, J. The effect of spatial heterogeneity in urban morphology on surface urban heat islands. *E&B 244*, **2021**, *111027*. https://doi.org/10.1016/j.enbuild.2021.111027.
13. Mutani, G.; Todeschi, V.; Matsuo, K. Urban Heat Island Mitigation: A GIS-based Model for Hiroshima. *Sustainability* **2019**, *11*, 2369. https://doi.org/10.3390/su11082369.
14. Todeschi, V.; Mutani, G.; Baima, L.; Nigra, M.; Robiglio, M. Smart Solutions for Sustainable Cities—The Re-Coding Experience for Harnessing the Potential of Urban Rooftops. *Appl. Sci.* **2020**, *10*, 7112. https://doi.org/10.3390/app10207112.
15. Mutani, G.; Beltramino, S. Geospatial assessment and modeling of outdoor thermal comfort at urban scale. *Sustain. Cities Soc.* **2022**, *77*, 103245. https://doi.org/10.1016/j.scs.2021.103245.
16. Xu, H.; Lin, D.; Tang, F. The Impact of Impervious Surface Development on Land Surface Temperature in a Subtropical City: Xiamen, China. *Int. J. Climatol.* **2013**, *33*, 1873–1883.
17. Scott, A.A.; Waugh, D.W.; Zaitchik, B.F. Reduced urban heat island intensity under warmer conditions. *Environ. Res. Lett.* **2019**, *14*, 094011.
18. Reis, C.; Lopes, A.; Santos Nouri, A. Urban heat island data by local weather types in Lisbon metropolitan area based on Copernicus climate variables dataset for European cities. *Sustain. Cities Soc.* **2021**, *65*, 102618.
19. Wang, W.; Wang, D.; Chen, H.; Wang, B.; Chen, X. Identifying urban ventilation corridors through quantitative analysis of ventilation potential and wind characteristics. *Build. Environ.* **2022**, *208*, 108759.
20. Lin, J.; Qiu, S.; Tan, X.; Zhuang, Y. Measuring the relationship between morphological spatial pattern of green space and urban heat island using machine learning methods. *Build & Envir 228*, **2023**, *109910*, https://doi.org/10.1016/j.buildenv.2022.109910.
21. Oliveira, A.; Lopes, A.; Niza, S.; Soares, A. An urban energy balance-guided machine learning approach for synthetic nocturnal surface Urban Heat Island prediction: A heatwave event in Naples. *Build. Environ.* **2021**, *195*, 107749. https://doi.org/10.1016/j.buildenv.2021.107749.
22. Liu, S.; Zhang, J.; Li, J.; Li, Y.; Zhang, J.; Wu, X. Simulating and mitigating extreme urban heat island effects in a factory area based on machine learning. *Sustain. Cities Soc.* **2021**, *70*, 102977. https://doi.org/10.1016/j.scs.2021.102977.
23. Espino, D.J.; Manchado, C.; Valcarce, A.R.; Moscardò, V. ArcUHI: A GIS add-in for automated modelling of the Urban Heat Island effect through machine learning. *Environ. Model. Softw.* **2022**, *146*, 105176. https://doi.org/10.1016/j.envsoft.2021.105176.
24. Mohammad, P.; Goswami, A.; Chauhan, S.; Nayak, S. Machine learning algorithm-based prediction of land use land cover and land surface temperature changes to characterize the surface urban heat island phenomena over Ahmedabad city, India Urban Climate 42, **2022**, 101116. https://doi.org/10.1016/j.uclim.2022.101116.
25. Wang, S.; Cai, W.; Tao, Y.; Sun, Q.C.; Wong, P.P.Y.; Huang, X.; Liu, Y. Unpacking the inter- and intra-urban differences of the association between health and exposure to heat and air quality in Australia using global and local machine learning models. *Sci. Total. Environ.* **2023**, *871*, 162005; ISSN 0048-9697.
26. Martini, A.F.; Pirulli, N. (a cura di). Torino: Storia di una città. Rivista TORINO. ISSN 2038-4068. Marzo 2011. MuseoTorino. Available online: http://www.museotorino.it/ (accessed on 5 January 2024). (In Italian)
27. Carlin, A.; Lo Verso, V.R.M.; Invernizzi, S.; Polato, A. Optimised daylighting for comfort and energy saving for the factory of the future. *Int. J. Mech. Control.* **2016**, *18*, 15–29.
28. Museo Torino. Scheda: Ex Stabilimento Teksid, ex Ferriere Fiat Vitali. Available online: https://www.museotorino.it/view/s/2ddd80eae7ca4555b51692f187cf20cd (accessed on 2 September 2023).
29. Museo Torino. Scheda: Ex Stabilimento Teksid, ex Ferriere Fiat Ingest. Available online: https://museotorino.it/view/s/a0886cd0a4924bde964799ca9952b297#:~:text=Lo%20stabilimento%2C%20collocato%20nell%27area%20compresa%20tra%20le%20vie,Urbana%20che%20ha%20trasformato%20l%E2%80%99area%20di%20Spina%203 (accessed on 5 January 2024).
30. QGIS STAC API Browser. Available online: stac-utils.github.io (accessed on20 July 2024).

31. Congedo, L. Semi-Automatic Classification Plugin: A Python tool for the download and processing of remote sensing images in QGIS. *J. Open Source Softw.* **2021**, *6*, 3172. https://doi.org/10.21105/joss.03172.
32. Mancino, G.; Ferrara, A.; Padula, A.; Nolè, A. Cross-Comparison between Landsat 8 (OLI) and Landsat 7 (ETM+) Derived Vegetation Indices in a Mediterranean Environment. *Remote Sens.* **2020**, *12*, 291. https://doi.org/10.3390/rs12020291.
33. Favretto, A. Urban Heat Island analysis with Remote Sensing and GIS methods: An application in the Trieste area (North-East of Italy). *Boll. Della Soc. À Geogr. Ital. Ser.* **2018**, *14*, 215–229. https://doi.org/10.13128/bsgi.v1i1.101.
34. Boehner, J.; Antonic, O. Land-surface parameters specific to topo-climatology. In *Geomorphometry—Concepts, Software, Applications*; Hengl, T., Reuter, H., Eds.; Elsevier: Amsterdam, The Netherlands, 2009; pp. 195–226. https://doi.org/10.1016/S0166-2481(08)00008-1.
35. Pereira, G.W.; Valente, D.S.M.; de Queiroz, D.M.; Coelho, A.L.d.F.; Costa, M.M.; Grift, T. Smart-Map: An Open-Source QGIS Plugin for Digital Mapping Using Machine Learning Techniques and Ordinary Kriging. *Agronomy* **2022**, *12*, 1350. https://doi.org/10.3390/agronomy12061350.
36. Guo, Q.; Su, Y.; Hu, T. LiDAR Data Filtering and Digital Elevation Model Generation. In *LiDAR Principles, Processing and Applications in Forest Ecology*; Guo, Q., Su, Y., Hu, T., Eds.; Academic Press: Cambridge, MA, USA, 2023; pp. 171–214. ISBN 9780128238943. https://doi.org/10.1016/B978-0-12-823894-3.00006-2.
37. Thompson, J.A.; Roecker, S.; Grunwald, S.; Owens, P.R. Digital Soil Mapping: Interactions with and Applications for Hydropedology. In *Hydropedology*; Lin, H., Ed.; Academic Press: Cambridge, MA, USA, 2012; pp. 665–709. https://doi.org/10.1016/B978-0-12-386941-8.00021-6.
38. Vermote, E.; Justice, C.; Claverie, M.; Franch, B. Preliminary Analysis of the Performance of the Landsat 8/OLI Land Surface Reflectance Product. *Remote Sens. Environ.* **2016**, *185*, 46–56. https://doi.org/10.1016/j.rse.2016.04.008.
39. Masek, J.G.; Vermote, E.F.; Saleous, N.E.; Wolfe, R.; Hall, F.G.; Huemmrich, K.F.; Gao, F.; Kutler, J.; Lim, T.K. A Landsat surface reflectance dataset for North America, 1990-2000. *IEEE Geosci. Remote Sens. Lett.* **2006**, *3*, 68–72. https://doi.org/10.1109/LGRS.2005.857030.
40. Kshetri, T. NDVI, NDBI & NDWI Calculation Using Landsat 7, 8. 2018. Available online: https://www.researchgate.net/publication/327971920_NDVI_NDBI_NDWI_Calculation_Using_Landsat_7_8 (accessed on).
41. McFeeters, S.K. The use of the Normalized Difference Water Index (NDWI) in the delineation of open water features. *Int. J. Remote Sens.* **1996**, *17*, 1425–1432. https://doi.org/10.1080/01431169608948714.
42. Ozelkan, E. Water Body Detection Analysis Using NDWI Indices Derived from Landsat-8 OLI. *Pol. J. Environ. Stud.* **2019**, *29*, 1759–1769. https://doi.org/10.15244/pjoes/110447.
43. Shastri, S.; Singh Prof Verma, P.; Rai, P.; Singh, A. Land Cover Change Dynamics and their Impacts on Thermal Environment of Dadri Block, Gautam Budh Nagar, India. *J. Landsc. Ecol.* **2020**, *13*, 1–13. https://doi.org/10.5775/fg.2020.063.i.
44. Jumari, N.A.S.K.; Ahmed, A.N.; Huang, Y.F.; Ng, J.L.; Koo, C.H.; Chong, K.L.; Sherif, M.; Elshafie, A. Analysis of urban heat islands with Landsat satellite images and GIS in Kuala Lumpur Metropolitan City. *Heliyon* **2023**, *9*, e18424. https://doi.org/10.1016/j.heliyon.2023.e18424.
45. Asdrubali, F.; Desideri, U. Building Envelope. In *Handbook of Energy Efficiency in Buildings*; Asdrubali, F., Desideri, U., Eds.; Butterworth-Heinemann: Oxford, UK, 2019; pp. 295–439. https://doi.org/10.1016/C2016-0-02638-4.
46. Rahman, M.N.; Rony, M.R.H.; Jannat, F.A.; Chandra Pal, S.; Islam, M.S.; Alam, E.; Islam, A.R.M.T. Impact of Urbanization on Urban Heat Island Intensity in Major Districts of Bangladesh Using Remote Sensing and Geo-Spatial Tools. *Climate* **2022**, *10*, 3. https://doi.org/10.3390/cli10010003.
47. He, C.; Shi, P.; Xie, D.; Zhao, Y. Improving the normalized difference built-up index to map urban built-up areas using a semi-automatic segmentation approach. *Remote. Sens. Lett.* **2010**, *1*, 213–221. https://doi.org/10.1080/01431161.2010.481681.
48. Hantzschel, J.; Goldberg, V.; Bernhofer, C. GIS-based regionalisation of radiation, temperature and coupling measures in complex terrain for low mountain ranges. *Meteorol. Appl.* **2005**, *12*, 33–42. https://doi.org/10.1017/S1350482705001489.
49. Čerba, O.; Charvát, K.; Janečka, J.; Jedlička, K.; Ježek, J.; Mildorf, T. The Overview of Spatial Data Harmonization Approaches and Tools. In Proceedings of the 4th International Conference on Cartography and GIS, Albena, Bulgaria, 18–22 June 2012.
50. Grasso, S. Isole di calore e Local Climate Zones. Verso un catalogo di azioni per la mitigazione e l'adattamento ai cambiamenti climatici (in Italian), Master di II Livello in "Metodi e Tecniche per il Governo di Territori Resilienti. Verso la gestione integrata dei rischi, Politecnico di Torino (In Italian). 2022.
51. Latini, A.; Gatti, L.; Giagnacovo, G.; Muleo, R.; De Rossi, P. Albedo Delle Superfici Vegetali e Benefici Dell'Inverdimento Urbano Nella Riduzione Dell'Isola di Calore Nelle Città. in Gli Ecosistemi Vegetali per la Rigenerazione Ecologica Delle Città, RT/2021/13/ENEA. 2021. Available online: https://iris.enea.it/retrieve/dd11e37d-0561-5d97-e053-d805fe0a6f04/RT-2021-13-ENEA.pdf (accessed on 20 July 2024).
52. Piano Paesaggistico Regionale della Regione Piemonte 2017. Available online: https://www.regione.piemonte.it/web/temi/ambiente-territorio/paesaggio/piano-paesaggistico-regionale-ppr (accessed on 5 January 2024). (In Italian)